Hydrogen transfer in excited pyrrole–ammonia clusters

O. David, C. Dedonder-Lardeux, C. Jouvet, H. Kang, and S. Martrenchard
Laboratoire de Photophysique Moléculaire du CNRS, Bât. 210 Université Paris-Sud, 91405 Orsay, France

T. Ebata
Department of Chemistry, Graduate School of Science, Tohoku University, Sendai 980-8578, Japan

A. L. Sobolewski
Institute of Physics, Polish Academy of Sciences, PL-02668 Warsaw, Poland

The excited state hydrogen atom transfer reaction (ESHT) has been studied in pyrrole–ammonia clusters $[\text{PyH}-(\text{NH}_3)_n + h\nu \rightarrow \text{Py}^\bullet + {}^\bullet\text{NH}_4(\text{NH}_3)_{n-1}]$. The reaction is clearly evidenced through two-color R2P1 experiments using delayed ionization and presents a threshold around 235 nm (5.3 eV). The cluster dynamics has also been explored by picosecond time scale experiments. The clusters decay in the 10–30 ps range with lifetimes increasing with the cluster size. The appearance times for the reaction products are similar to the decay times of the parent clusters. Evaporation processes are also observed in competition with the reaction, and the cluster lifetime after evaporation is estimated to be around 10 ns. The kinetic energy of the reaction products is fairly large and the energy distribution seems quasi mono kinetic. These experimental results rule out the hypothesis that the reaction proceeds through a direct N–H bond rupture but rather imply the existence of a fairly long-lived intermediate state. Calculations performed at the CASSCF/CASMP2 level confirm the experimental observations, and provide some hints regarding the reaction mechanism. © *2004 American Institute of Physics.* [DOI: 10.1063/1.1704639]

I. INTRODUCTION

In the past few years, it has been demonstrated that the excited state dynamics of phenol–ammonia clusters is not governed by an excited state proton transfer in an acid–base mechanism as previously assumed. In contrast, it is controlled by a radical reaction namely the hydrogen transfer process.[1–5] Indeed, this reaction leads to the formation of neutral $\text{NH}_4(\text{NH}_3)_n$ clusters which are metastable (μs lifetimes) and can easily be ionized with low energy photons. The same excited state hydrogen transfer reaction has been also observed in indole and methylindole clustered with ammonia.[3,5,6]

The results of *ab initio* electronic-structure calculations performed by Sobolewski and Domcke provide strong evidence for a surprisingly simple and general picture of the H transfer mechanism in aromatic enol and azine molecules.[7–10] The key role in this picture is played by an excited singlet state of $\pi\sigma^*$ character, which has a repulsive potential-energy function with respect to the stretching of O–H or N–H bonds. In the isolated molecules, the $^1\pi\sigma^*$ potential-energy function intersects not only the bound potential-energy functions of the excited $^1\pi\pi^*$ state, but also that of the electronic ground state. Through the conical intersections with the $^1\pi\pi^*$ state and the ground electronic state, the $^1\pi\sigma^*$ state triggers an ultrafast internal-conversion process. In protic solvents, the $^1\pi\sigma^*$ state promotes a hydrogen-transfer process from the chromophore to the solvent. In the case of ammonia clusters with a chromophore, the $^1\pi\sigma^*$ state leads to the formation of neutral solvated ammonium radicals $\text{NH}_4(\text{NH}_3)_m$.

Pyrrole ($\text{C}_4\text{H}_5\text{N}$ that we will abbreviated as PyH) is a building block in many important molecules of biological interest. It is a five-membered heterocyclic aromatic ring in which the lone electron pair on the N atom and the two double bonds of the aromatic ring form a delocalized π bond. Heckman first reported in 1958 that PyH exhibits no emission of light neither fluorescence nor phosphorescence.[11] Since then, many experimental and theoretical studies on PyH have been performed to understand its electronic structure and photochemical properties.[12–14]

Recently, Sobolewski and Domcke have calculated that in PyH the dissociative $\pi\sigma^*$ state is lower than the $\pi\pi^*$ state, in agreement with the experiments of photofragment translational spectroscopy where the formation of H atoms and the corresponding pyrrolyl radicals are detected.[15,16] The observation of a fast H atom with a nearly monokinetic translational energy distribution is a good evidence that UV excitation of PyH leads directly to the dissociative $\pi\sigma^*$ state. PyH should then be the simplest molecule to study the H transfer reaction because it involves direct excitation to the $\pi\sigma^*$ dissociative state, a case much simpler than phenol or indole where the excitation is primarily localized on the $\pi\pi^*$ state and transferred to the $\pi\sigma^*$ state through a conical intersection before the reaction can proceed.

The purpose of this paper is first to evidence the H transfer reaction in PyH–ammonia clusters via detection of the $\text{NH}_4(\text{NH}_3)_m$ products, second to determine the reaction rate and third to evaluate the kinetic energy released in the reaction. More specifically we want to address the question of the mechanism that leads to fragment ejection: the $\text{NH}_4(\text{NH}_3)_m$ radical products must be ejected from the initially excited $\text{Py}-\text{H}(\text{NH}_3)_n$ clusters in order to be observed experimen-
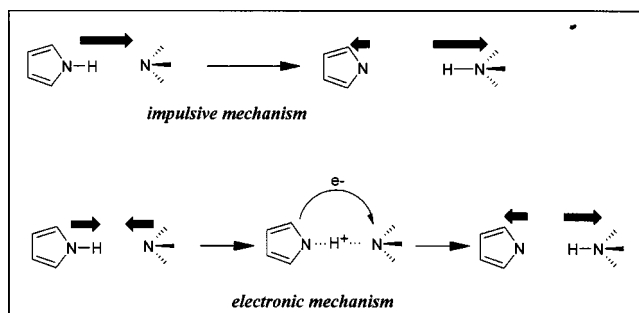
FIG. 1. Possible mechanisms for ejection of radical products from the parent clusters. The upper part of the figure represents the impulsive mechanism: excitation leads to the $\pi\sigma^*$ repulsive state. The H atom is ejected with a lot of kinetic energy and collides with the nearest NH_3 molecule. The lower part of the figure represents the electronic mechanism: the repulsion starts after the concerted electron and proton transfer from pyrrole to the ammonia cluster. The repulsion between Py (pyrrolyl) radical and the solvated ammonium radical is induced by the diffuse character of the Rydberg-type electron cloud.

tally, otherwise ionization of the $PyH^* - (NH_3)_n$ parent clusters—which may have the isomeric form $Py^\bullet - {}^\bullet H - NH_3(NH_3)_{n-1}$—would lead to the observation of $[Py^\bullet - {}^\bullet H - NH_3(NH_3)_{n-1}]^+$ cluster ions and not to the observation of $NH_4(NH_3)_m^+$ ions, at least under controlled experimental conditions as will be explained in the Results. What is the driving force leading to the radical production and what is its mechanism? We will discuss two limiting cases as presented in Fig. 1.

The simplest reaction path is the ejection of the H atom from the $PyH\,{}^1\pi\sigma^*$ excited state within the cluster, with a nearly monokinetic energy (of ~ 0.8 eV in the case of PyH excited at 243 nm), followed by collision of this H atom with the nitrogen atom of the nearest NH_3 molecule, hydrogen bonded to the pyrrolic N–H bond. In such a reaction scheme, the initial kinetic energy of the ejected H atom is randomized into the vibrational, rotational and translational degrees of freedom of the $NH_4(NH_3)_m$ radical product. The translational energy is finally converted in kinetic energy separating the $NH_4(NH_3)_m$ cluster from the pyrrolyl radical ($Py^\bullet$). This mechanism will be called "impulsive mechanism."

Another possibility is that after electronic excitation, a charge-transfer induced proton transfer occurs, resulting in formation of the $Py^\bullet \cdots {}^\bullet NH_4(NH_3)_m$ cluster. The preliminary step of the reaction involves compression of the $N\cdots N$ bond which reduces (or eliminates) the barrier for the reaction. The Rydberg-type nature of the $NH_4(NH_3)_m$ radical cluster results in repulsion of the cluster from the pyrrolyl radical. We will call this mechanism "electronic mechanism."

II. EXPERIMENT

The experiments have been conducted partly in Photophysique Moléculaire (Orsay, France) for nanosecond experiments, kinetic energy measurements, and picosecond decays of the parent clusters and partly in Tohoku University (Sendai, Japan), where the risetimes of the solvated ammonium products have been measured together with the PyH–ammonia decay times on the picosecond time scale.

A. The Orsay setup

PyH–ammonia clusters are produced by expanding a mixture of NH_3 and PyH seeded in helium through a pulsed valve. The gas mixture is obtained in passing the premixed $He/NH_3(0.5\% - 2\%)$ gas flow over a reservoir containing room temperature PyH. The backing pressure is varied between 0.5 and 3 bar and the nozzle diameter is 300 μm. The jet is skimmed before entering the time of flight mass spectrometer (Jordan Co.), between the extraction electrodes, which are separated by $\frac{1}{2}$ in., where the clusters are ionized. The ions are then accelerated between two other electrodes also separated by $\frac{1}{2}$ in. before flying in the 1 m field free region (grounded). The ions are detected by microchannel plates, the signal is amplified and recorded on a LeCroy 9400 oscilloscope.

The mass spectrometer can also be run in reflectron mode when high resolution mass spectra are necessary: in that case, after the 1 m field free region, the ions are reflected by a series of electrodes and fly another 1 m before being detected by a second pair of microchannel plates.

In the pulsed extraction mode used for kinetic energy release measurements, the mass spectrometer works in the direct mode and high voltages (1000 and 750 V) are switched on the lower and upper extraction electrodes with a Behlke high voltage switch. This method has been already demonstrated,[17] where we set a long waiting time between the excitation/ionization lasers and the ion extraction pulses to allow the initially produced ion cloud to be broadened if some kinetic energy is released in the reaction. This method is sensitive to the dispersion of the ion cloud along the TOF axis, in our case the vertical axis. The ions which will be located near the lower electrode are more accelerated than the ones nearby the upper one, they will travel faster in the field free region of the TOF and will arrive on the detector at earlier times. Practically, when the delay between the laser and the extracting field is increased, the excitation/ionization position between the two extraction plates is varied by translating the lens upstream the jet axis so that the ions can reach the detector. To get rid of the initial width of the mass peaks, due to the finite size of the lasers and to the distribution of velocities in the jet, the variation of the peak width (Δw) can be measured as a function of the delay (Δt) between laser and pulsed extraction field: there is a linear variation of Δw vs Δt and the resulting slope, divided by a calibration parameter, gives a direct measure of the velocity.

Two different laser setups have been used for cluster excitation and ionization:

(i)   For the experiments running in the nanosecond time scale, we used a frequency doubled excimer pumped dye laser for the cluster excitation; and the third (355 nm, 3.5 eV) or fourth harmonic (266 nm, 4.66 eV) of a Nd:YAG, delayed by a few hundred ns, was the ionization probe.

(ii)   For time resolved experiments, a home made picosecond OPO laser system was used.[18] The picosecond pulses are produced with a Nd:YAG laser through a combination of saturable absorber and passive negative feedback; a macro-impulsion involving 50 pulses

of 10 ps duration, separated by 10 ns, is produced at a 20 Hz repetition rate. Seventy percent of the 1.064 μm pump power, e.g. 800 mW, is frequency tripled to 355 nm (220 mW) to pump synchronously a BBO-based visible OPO laser tunable from 410 to 750 nm. The present experiment makes use of the latter visible OPO output around 450 nm which is further frequency doubled to excite the S_0-S_1 transition. A portion of the frequency tripled 355 nm is optically delayed and used as the ionization probe laser. The spectral width of the visible OPO is less than 3 cm^{-1}. The laser characteristics make it possible to monitor dynamical processes with a resolution of 12 ps, if the reactive system can relax within 10 ns corresponding to the laser pulse separation. The multipulse structure precludes, however, the risetime measurement of stable species [in our case $NH_4(NH_3)_m$]. In the wavelength region used here, time zero and the cross correlation of the laser pulses have been measured either with anisole or dimethylaniline: these molecules when excited at 225 nm and ionized with 355 nm give rise to a steplike pump/probe signal that can be fitted with an erf function (integral of a Gaussian function). The assumption underlying this fit is that the laser pulses are Gaussian so that the width parameter introduced in the erf function represents the cross correlation of the lasers. The value obtained under these conditions is 11.7$\pm$1.3 ps.

B. The Tohoku setup

The experimental setup of the Tohoku University is essentially the same as in Orsay, with the main differences concerning the mass spectrometer and the picosecond laser. Briefly, a frequency tripled output (355 nm) of a mode-locked picosecond Nd^{3+}:YAG laser (Ekspra PL2143B) is introduced into an OPG/OPA system (Ekspra PG401SH) for a tunable UV light generation. Typical bandwidth and output power of the UV light is 10 cm^{-1} and 50–100 μJ, respectively. Part of the 355 nm output is used as the ionization light source. The laser operates at 10 Hz repetition rate and its pulse width is estimated to be ~12 ps. The pulse widths of the tunable UV and 355 nm picosecond laser pulses are obtained by a cross correlation measurement using two-photon resonant three photon ionization of NH_3 in the supersonic beam. When the wavelength of the tunable UV pulse is 248 nm, the energy corresponding to the sum of one 248 nm photon + one 355 nm photon is resonant with the $C'(v_2=5)-X(v_2=0)$ transition[19] of NH_3, where C' is the $3p$-Rydberg state and v_2 is the umbrella mode of NH_3. By scanning the delay time of the 355 nm pulse with respect to the 248 nm pulse while monitoring the NH_3^+ ion, we obtain the cross correlation curve which can be well fitted to a Gaussian function of 12.4–0.2 ps width. The laser beams are introduced into the vacuum chamber and cross the molecular beam of PyH/ammonia diluted in helium. A computer controlled optical delay line set the delay time between the tunable UV and the ionization laser pulses.

Jet-cooled PyH–ammonia clusters are generated by a supersonic expansion of PyH/ammonia gaseous mixture seeded in helium carrier gas (typically 3 bar) into vacuum through a pulsed nozzle (General valve) with a 0.8 mm aperture. The free jet is skimmed by a skimmer having a 0.8 mm diam (Beam dynamics) located 30 mm downstream of the nozzle. The UV lasers cross the supersonic beam 50 mm downstream of the skimmer. The clusters or product ions are extracted in the direction perpendicular to the plane of the molecular beam and the laser beams. The ions are then mass analyzed in a 50 cm time-of-flight tube and detected by an electron multiplier (Burle 4700). The ion signals are integrated by a boxcar integrator (Par model 4420/4400) connected to a computer.

III. COMPUTATIONAL DETAILS

The CASSCF calculations[20] of the potential-energy surface (PES) relevant for the photophysics of the PyH–ammonia cluster in the $^1\pi\sigma^*$ state were performed in Warsaw. In the calculations, the $N_{Py}N_{am}$ (N···N) and $N_{Pyr}H$ (N–H) were frozen at fixed values while the remaining intra- and intermolecular degrees of freedom of the cluster were optimized under the imposed constrains of the C_s symmetry. Thus the calculated two-dimensional PES represents a CASSCF minimum-energy surface spanned by N···N and N–H stretching coordinates. To account for dynamical electron correlation effects, which are largely neglected at the CASSCF level, single-point calculations at the MRMP2 level[21] (multireference second-order Møller–Plesset perturbation theory with respect to the CASSCF reference) were performed at the most crucial points of the $^1\pi\sigma^*$ PES.

In the calculations the standard 6-31G(d,p) split-valence Gaussian basis set with polarization functions on all atoms was augmented with standard diffuse functions on nitrogen atoms and on hydrogen atom of PyH. Anticipating that the biradical possesses Rydberg character, the basis set was supplemented with an additional set of diffuse s and p Gaussian functions of exponent $\xi=0.02$ on the nitrogens. The active space in the CASSCF and MRMP2 calculations includes five π orbitals of PyH and the lowest unoccupied (in the Hartree–Fock reference) σ^* orbital. The basis set as defined above was also used in the MP2 optimization of the ground-state geometry. All calculations were performed with the GAMESS program package.[22]

IV. RESULTS

A. Evidence for the hydrogen transfer reaction using nanosecond lasers

The method to evidence the H transfer mechanism is based on the particular properties of ammonia clusters: $(NH_3)_n$ clusters can trap a H atom and produce solvated ammonium clusters $NH_4(NH_3)_m$. Besides, the $NH_4(NH_3)_m$ radical clusters are sufficiently long lived to allow an efficient detection by ionization with delayed nanosecond laser pulses [lifetimes measured to be 3 and 7 μs for $n=1$ and 2, respectively, whereas NH_4 is a very short-lived species (15 ps Ref. 23)], and their ionization potentials (I.P.) are low[24] so that the 355 nm (3.5 eV) laser light can be used to probe the

$NH_4(NH_3)_m$—radical products with $m \geq 2$. The NH_4NH_3 radical was probed by the fourth harmonic of the Nd:YAG laser (266 nm, 4.66 eV).

It is very important to prove that the reaction observed is the H transfer reaction (ESHT) in the excited state and not the excited state proton transfer (ESPT) reaction nor a reaction in the ionized clusters. Indeed, the $NH_4^+ (NH_3)_m$ cation signal observed in the phenol–ammonia system has long been attributed to an excited state proton transfer followed by evaporation in the ionized species.[5,25] However, there is no ambiguity when a long delay is fixed between excitation (pump) and ionization (probe): in this case, ionization takes place at different time and position in the jet from those of excitation, therefore when the probe laser (355 nm or 266 nm) is triggered a few hundred ns after the pump laser, the parent excited state species have already either reacted or relaxed to the ground state. Only long lived species such as neutral reaction products or triplet states can be ionized by the probe laser and therefore one can discriminate between excited state proton transfer reaction and H transfer reaction. In the classical model for excited state proton transfer reaction,[5,25] the initially excited $[MH^*-(NH_3)_n]$ cluster converts to the excited charge transfer species $[M-NH_4^+(NH_3)_{n-1}]^*$ which is stable with respect to dissociation in two ions, and will relax to its ground state during the time between pump and probe lasers.

In the same way, to insure that $NH_4(NH_3)_m^+$ are not produced by an ionic reaction, i.e. from ions produced by two photons of the pump laser and absorbing one more probe photon to react, an extraction voltage of 250 V is applied continuously on the two first plates of the mass spectrometer during the delay between the pump and the probe lasers so that the ions produced by the first laser (pump) are repelled from the jet axis before they can be excited by the probe laser. Let us mention here that these ions will be detected (but at shorter flight times than the ions issued from a two-color process) as long as the pump laser displacement upstream the jet is small enough to let them reach the detector (a 1 μs delay between the lasers corresponds to a 1.5 mm displacement of the pump laser with respect to the spectrometer axis, which is negligible as compared to the 25 mm size of the microchannel plates).

The results of such an experiment carried out with a nanosecond Nd:YAG laser are shown in Fig. 2. In a one-color experiment with excitation and ionization at 225 nm (5.51 eV), both the parent and fragment ions are observed [Fig. 2(a)], which already indicates that the reaction is faster than the laser pulse, i.e. 10 ns. When the 355 nm probe laser is added with a pump/probe delay of 1 μs [Fig. 2(b)], the one-color signal is still present but the delayed two-color signal on $NH_4^+(NH_3)_{m-2}$ clusters (indicated by arrows in Fig. 2) is much larger while the parent ions are not observed: the excited $PyH^*-(NH_3)_n$ clusters have either reacted or relaxed to their ground state.

When 266 nm is used as a probe laser, the NH_4NH_3 ions are also greatly enhanced. This is the result expected if the $NH_4(NH_3)_m^+$ ions come from ionization of neutral radicals since NH_4NH_3 can be ionized with the 266 nm probe laser but not with 355 nm (I.P.=3.88 eV). It indicates that the H
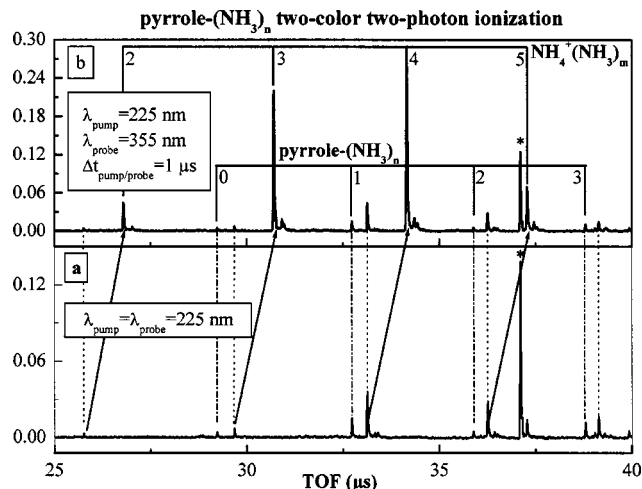

FIG. 2. Mass spectra recorded with $\lambda_{pump}=225$ nm and $\lambda_{probe}=355$ nm for pyrrole–$(NH_3)_n$ clusters. (a) Mass spectrum recorded with the 225 nm laser alone, PyH–$(NH_3)_n$ and $NH_4(NH_3)_m$ clusters are weakly observed. (b) Mass spectrum recorded with the pump laser at 225 nm, the probe laser at 355 nm, and a delay $\Delta t_{pump/probe}=1$ μs between the two lasers. The flight times of the ions produced through two-color ionization (late ions) are thus 1 μs longer than those of ions produced by one-color only (prompt ions), which is shown by the full arrows. In the two-color experiment, the $NH_4(NH_3)_m$ ion signal is much greater than the one-color signal (the intensity scale for spectrum 2 is twice that of spectrum 1) while no signal is detected on the PyH–$(NH_3)_n$ cluster masses. The excited clusters have either reacted or decayed to the ground state during the 1 μs pump/probe delay. The asterisk indicates anisole ions: anisole was added in the jet to find time $t=0$ between pump and probe lasers. Experimental conditions: backing pressure $P_0=2.3$ bar, pyrrole at room temperature, carrier gas 2% NH_3 in helium, laser intensities were 40 μJ/pulse for 225 nm and 2 mJ/pulse for 355 nm.

transfer reaction already takes place in $PyH-(NH_3)_2$. $PyH-(NH_3)_n$ cluster ions are detected in one-color two-photon ionization with the 266 nm laser but the reaction products are not observed, which already tells that the reaction threshold lies between 266 and 225 nm (4.66 and 5.51 eV).

The results of these two-color two-photon delayed ionization experiments clearly demonstrate that we are dealing with the H transfer reaction and not with the excited state proton transfer nor with a reaction in ionized clusters.

B. Picosecond dynamics

1. Excitation energy dependence of the reaction

Let us mention first that femtosecond experiments have been tried on this system using the DRECAM/SPAM setup[26] with two excitation wavelengths, the third (266 nm) and the fourth (200 nm) harmonics of the titanium sapphire laser, but no dynamics could be recorded.

Using the picosecond laser, we could scan the excitation energy from 266 up to 220 nm. No reaction is observed when the excitation wavelength is longer than 235 nm (photon energy below 5.3 eV). In particular, the experiment could not be achieved either at 248 or at 243 nm, the wavelengths used to study the kinetic energy of the H atom produced in the photodissociation of free PyH.[15,16]
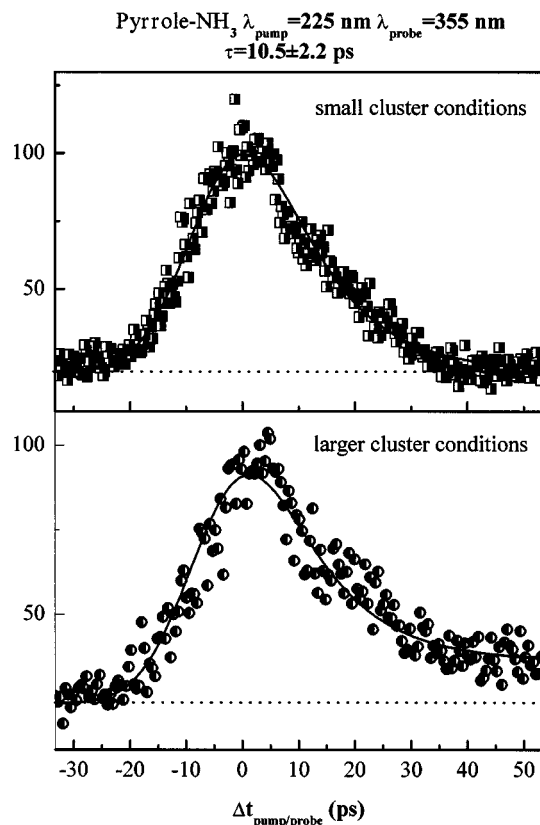
FIG. 3. Pump/probe picosecond transients recorded on the pyrrole–NH$_3$ mass. (Top) Small cluster distribution, the signal decreases back to the background for delays larger than 35 ps. (Bottom) Larger cluster distribution: in this case, a signal remains present at long delay between pump and probe lasers that evidences an evaporation process. These pump/probe transients have been obtained with the bunched picosecond laser in Orsay, with laser intensities of 15 μJ/pulse at 225 nm and 500 μJ/pulse for 355 nm.

2. Cluster lifetimes

The pump/probe decays observed for the parent ions are presented in Fig. 3 with different cluster size distributions. Under small cluster size conditions, the 1−1 cluster is almost exclusively produced, and its decay, at our time resolution, is essentially a single exponential. The lifetime of the 1−1 cluster is in the order of $\tau_1 = 10.5 \pm 2.2$ ps, close to the shortest lifetime which can be determined with the present system (Fig. 3, top).

Under conditions where larger size clusters are present, the signal does not come back to 0 at long delay, as can be seen in Fig. 3, bottom panel. The change of the decay signal with the cluster distribution is a clear indication that evaporation processes occur.[17] Such evaporation processes give rise to a steplike function in addition to the exponential decay.

Under these conditions, the lifetime of larger clusters can be measured. In fact only the 1−2 and 1−3 cluster lifetimes could be recorded, the 1−4 cluster mass being too close from the PyH dimer mass to be measured cleanly. The lifetime increases as the cluster size increases being $\tau_2 = 13 \pm 3$ ps for PyH−(NH$_3$)$_2$ and $\tau_3 = 24 \pm 8$ ps for the PyH−(NH$_3$)$_3$.

Using the setup at Tohoku University, it has been possible to measure both the decay times of PyH−(NH$_3$)$_n$ clusters and the appearance time for the NH$_4$(NH$_3$)$_m$ products
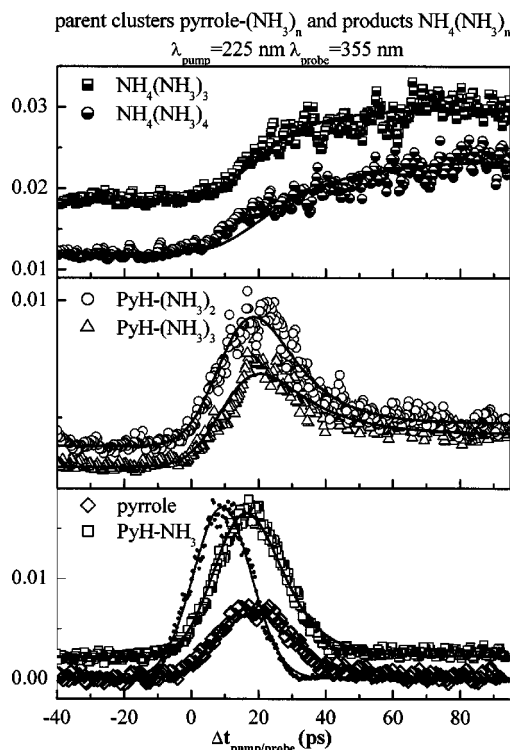

FIG. 4. Pump/probe picosecond transients recorded on the pyrrole–(NH$_3$)$_n$ cluster masses and on the NH$_4$(NH$_3$)$_m$ reaction products. (Bottom) Decays observed for pyrrole (diamonds) and PyH–NH$_3$ (squares). The lines correspond to single exponential fits with $\tau_1 = 9.5 \pm 1.5$ ps. The autocorrelation function of the lasers is represented in small black dots with its Gaussian fit in dashed lines. (Middle) PyH–(NH$_3$)$_2$ (circles) and PyH–(NH$_3$)$_3$ (triangles) decay curves. Single exponential fits give $\tau_2 = 12.1 \pm 1.5$ ps and $\tau_3 = 15.3 \pm 2$ ps, respectively. (Top) Transients recorded on the reaction products NH$_4$(NH$_3$)$_3$ (half-filled squares) and NH$_4$(NH$_3$)$_4$ (half-filled circles). The transients are fit by an exponential growth with $\tau_3' = 18 \pm 6$ ps and $\tau_4' = 22 \pm 6$ ps. These pump/probe transients have been obtained with the picosecond laser in Sendai. The autocorrelation function of the laser was recorded using two-color ionization of NH$_3$ with pump at 245 nm and the probe at 355 nm and was fit with a Gaussian function of 12 ± 0.6 ps width. The laser intensities are 10 μJ/pulse at 225 nm and 1 mJ/pulse for 355 nm.

with $m = 3$ and 4, as shown in Fig. 4. The decay times observed in Tohoku ($\tau_1 = 9.5 \pm 1.5$, $\tau_2 = 12.1 \pm 1.5$, $\tau_3 = 15.3 \pm 2$) are slightly shorter than those measured in Orsay, but the values fall within the experimental errors, and the observed appearance times (Fig. 4 top panel) for the NH$_4$(NH$_3$)$_{3,4}$ products, $\tau_3' = 18 \pm 6$ ps and $\tau_4' = 22 \pm 6$ ps, are, within the experimental error, similar to the decay of the parent clusters.

3. Long lifetime component

The underlying step function (in large cluster condition) has been observed both in the Orsay and Tohoku University setup. In Tohoku University, the decay of the long lifetime component could not be seen (it looked as a plateau), which means that the clusters undergoing evaporation have lifetimes longer than 1 ns. On the other hand, the laser system in Orsay is constituted by a bunch of 50 impulsions separated by 10 ns, which enabled us to estimate the long component lifetime.

Building up of the pump/probe signal with a bunched laser   **pump/probe signal observed during a scan of the delay line**
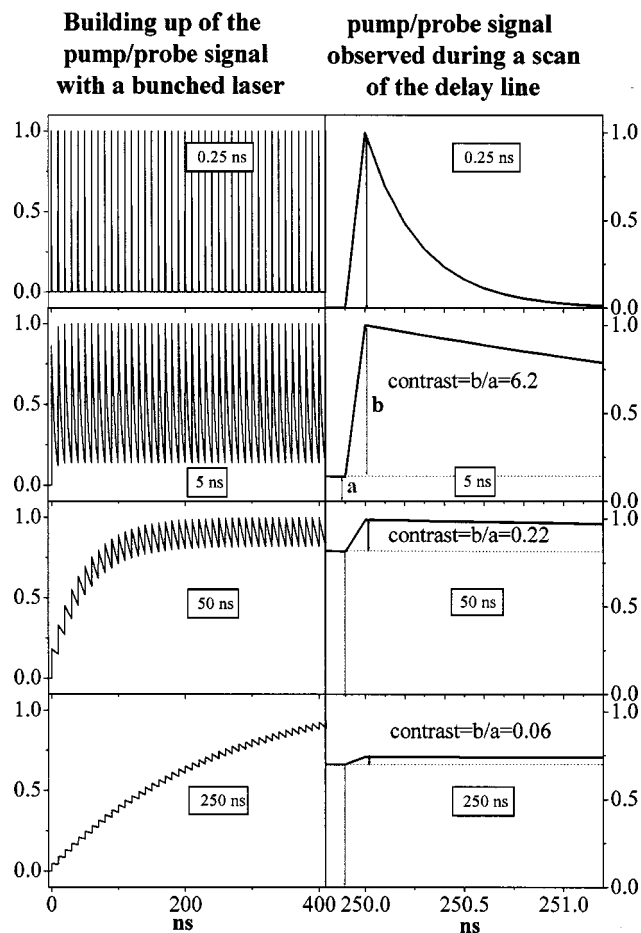

FIG. 5. Simulation of the contrast in the pump/probe experiment as a function of the lifetime of the process for a bunched picosecond laser composed of 50 micropulses of 10 ps separated by 10 ns. Upper left panel: the lifetime is 250 ps the signal returns to 0 before the next pulse. The right part of the figure presents an enlarged view of the signal for one micropulse, and mimics what is recorded on the digital oscilloscope; the lower panels present the cases of different decay times: for a 5 ns decay, the contrast defined in the right panels is very good (6.2), whereas when the lifetime is 100 ns the contrast is very poor (0.06). For an infinite lifetime, the contrast is given by the inverse of the number of pulse (1/50) and cannot be observed properly due to the fluctuation of the laser intensity. For a rising signal (reaction products) as presented in the lower panels, the contrast is always very poor, well within the noise due to the fluctuation of the laser intensity, whatever the value of the time constant. This completely precludes the measurement rise times [in our case the appearance times of the $NH_4(NH_3)_m$ reaction products].
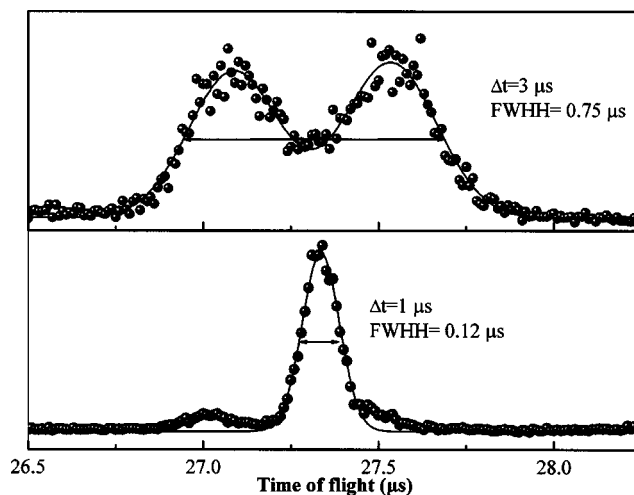

FIG. 6. Evolution of the mass peak width as a function of the delay between the laser and the extraction pulse of the mass spectrometer. The mass observed is $M = 86$ ($NH_4(NH_3)_3$).

The evolution of the pump/probe signal with a bunched picosecond laser is represented for different decay times in Figs. 5(a) and 5(b). The figure presents the building up of the signal as a function of time e.g. the number of micropulses. If the species observed decays rapidly, i.e. with a lifetime of less than 500 ps, the pump/probe signal due to one micropulse decays to zero before the next micropulse arrives, 10 ns afterwards [Fig. 5(a), upper panel]. At the opposite, if the decay is long, the pump/probe signal has not completely decayed before the next micropulse arrives, and this effect leads to an apparent background signal. The intensity of this background is related to the lifetime as can be observed in Fig. 5(a). As an example, for a 5 ns lifetime process, the intensity of the signal when the probe laser is triggered before the pump laser (before $t = 0$) represents 16% of the sig-

nal maximum recorded at $t = 0$. The contrast, defined as the ratio between the signal observed when the probe laser is triggered before the pump laser ($t < 0$) and the signal intensity at $t = 0$ is $C = 6.2$ [see Fig. 5(a) right panels]. When the lifetime increases, the contrast decreases (down to 0.06 for a 250 ns lifetime), and for an infinite lifetime it will be proportional to the inverse of the number of pulses in the bunch (typically $C = 1/50 = 0.02$), which is less than the fluctuation of the laser and is hence not measurable. For the same reason, rise times cannot be measured with such a laser as can be seen in Fig. 5(b).

The measure of the contrast (as defined in the previous paragraph) in the decays recorded for $PyH-(NH_3)_n$ can be then used to estimate the long component lifetime. The values obtained are not very precise (for $n = 1, 2$ $C > 1$, for $n = 3$ $C = 1$ to 2) but the most important fact is that one can deduce that the long component has a lifetime less than 10 ns for the 1–1 and 1–2 clusters and in the order of 10 ns for the 1–3. After evaporation the excited clusters are still decaying in the ns range.

C. Kinetic energy measurement

As stated in the experimental section, the kinetic energy release in the reaction can be measured in using the mass spectrometer in the direct mode and pulsing the extraction voltages on the lower and upper extraction electrodes. If we set a long delay time between the excitation/ionization lasers and the ion extraction pulses, the initially produced ion cloud has the time to broaden whenever some kinetic energy is released in the reaction. An example of the change of the mass peak shape as a function of the delay between the lasers (excitation and ionization) and the pulsed extraction field of the mass spectrometer is given in Fig. 6. At longer delay times between the lasers and the extraction pulse, the peak broadens and splits into two Gaussian-type peaks. The broadening of the peak is a clear indication of the fast velocity of the reaction products. From the calibration of the mass

spectrometer[17] and assuming a monokinetic energy distribution, the velocity of the outgoing reaction products can be measured.

The assumption of a monokinetic energy distribution is substantiated by the appearance of a dip in the center of the peak at longer delay times. This dip in the middle of the peak can be explained in the following way: for a monokinetic energy distribution, the ions will be on the surface of a sphere that will enlarge as it travels to the detector (30 μs). The ions which have an initial velocity along the spectrometer axis (vertical axis) will be detected at short or long times depending on the direction of their velocity while those that have an initial velocity perpendicular to the detection axis should be detected in the center of the peak. But if the ion cloud becomes too large, it will spread beyond the area of the detector which is only 2.5 cm in diameter and these latter ions will be lost leading to a dip in the center of the mass peak. In the case of a statistical energy distribution, the ions will have a kinetic energy varying between 0 and E_{max} (available energy) and will then be present in all the volume of the expanding sphere. In that case only a small part of the ions having their initial velocity perpendicular to the spectrometer axis will be lost when the ion cloud gets too large, and the mass peak should retain a Gaussian-type shape.

Let us mention that we do not expect any anisotropy in the kinetic energy distribution, because the typical reaction times measured (10–30 ps for large clusters) are longer than the rotational period: for a cluster temperature in the jet around 25 K, and a calculated rotational constant of 1.3 $\times 10^{-3}$ cm^{-1} for PyH–(NH$_3$)$_3$, the mean rotational level is $J=25$ and the rotational period of the order of 1 ps.

Under this assumption of monokinetic energy release, the measured velocities are 1030 ± 100, 930 ± 50, and 760 ± 30 m/s for NH$_4$(NH$_3$)$_m$ with $m=2$, 3, and 4, respectively, which correspond to total kinetic energies $E_{kin}=0.52 \pm0.10$, 0.64 ± 0.07, and 0.60 ± 0.05 eV for about 1.5 eV of available energy.[16]

## D. Theoretical results

The minimum-energy PES of the $^1\pi\sigma^*$ state of the PyH–ammonia cluster is shown in Fig. 7(a). In the calculation the N$\cdots$N and N–H distances were varied in the range of 2.2–3.2 Å and 0.8–2.2 Å, respectively, with the interval of 0.2 Å. The figure shows the surface up to 1 eV plotted with contour lines of 0.1 eV. Two apparent minima of the PES (abbreviated by 2 and 4 in the figure) separated by a barrier (3) are clearly visible. The values of the N$\cdots$N and N–H distances and energies of the structures are collected in Table I. At the CASSCF level the local minimum (2) is higher by about 0.5 eV than the global minimum (4).

At this level of theory the local minimum (2) is separated from the global minimum (4) by a barrier of only 0.04 eV. Dynamical electron correlation included at the MRMP2 level has almost no effect on the relative energy of the two minima, but eliminates the barrier between them (Table I). It is thus very likely, that PES surface of the $^1\pi\sigma^*$ state of the PyH–NH$_3$ cluster has only a single minimum with respect to the hydrogen transfer reaction. The expected motion of the

(a)

| Structure 1 | Structure 3 | Structure 4 |
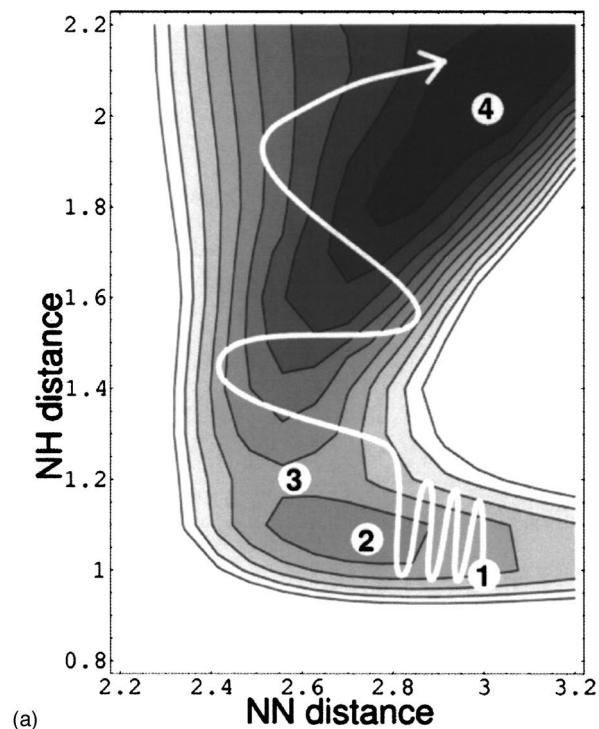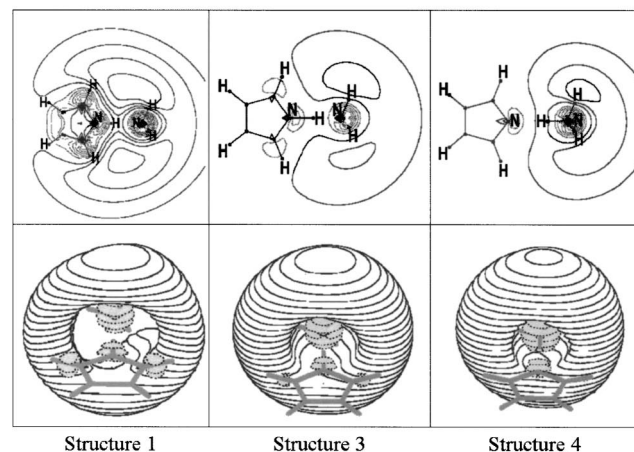
(b)

FIG. 7. (a) Calculated potential energy surface at the CASSCF level for PyH–NH$_3$. The contours are separated by 0.1 eV. The coordinates plotted are: horizontal axis N$\cdots$N distance (between the pyrrolic nitrogen and the ammonia nitrogen, vertical axis pyrrolic N–H distance (between the hydrogen atom and the pyrrolic N). A vertical excitation from the ground state geometry leads to region 1 where there is a high barrier for the hydrogen transfer. When the N$\cdots$N distance decreases, as the system goes down the entrance valley, there is a local minimum 2 along the reaction path, and the barrier to H transfer decreases considerably. After the barrier 3, the system evolves rapidly to dissociation in a radical pair 4. (b) Representation of the σ^* orbital along the reaction path in two and three dimensions: in the entrance channel, at the ground state geometry 1, the σ^* orbital extends over the whole complex and has a bonding nodal pattern between the particular shells localized on molecular units, with the H atom still bound to pyrrole, the orbital can thus be classified as the bonding with respect to the intermolecular interaction and results in contraction of the N$\cdots$N distance. At the transition state 3, there is an electron transfer to the solvent while the hydrogen atom is still linked to pyrrole, although the N–H bond has started to stretch. In the exit channel, proton transfer neutralizes the system leading to the ESHT reaction and the σ^* orbital localizes almost exclusively on the ammonium with an antibonding nodal pattern with respect to the pyrrolyl radical. This will result in dissociation of the complex that is now a radical pair with a large Rydberg orbital localized on the hydrogenated solvent.

TABLE I. CASSCF and CASMP2 relative energy (in eV) of the $^1\pi\sigma^*$ state of the pyrrole–ammonia complex calculated at the MP2 geometry of the ground state (1), at the CASSCF geometry of the local minimum (2), at the geometry of the global minimum (4) of the $^1\pi\sigma^*$ potential energy surface and at the transient structure between them (3). The N–H and N$\cdots$N distances of the optimized structures are given in angstroms.

Structure	N–H	N$\cdots$N	CASSCF	CASMP2
1, vertical excitation from the ground state equilibrium geometry	1.021	3.013	0.849	0.756
2, $\pi\sigma^*$ (local minimum at the CASSCF level in the entrance valley)	1.060	2.750	0.533	0.488
3, $\pi\sigma^*$ (transient structure between the entrance and the exit valleys)	1.2	2.6	0.571	0.386
4, $\pi\sigma^*$ (global minimum in the exit valley)	1.996	3.022	0	0

wave packet on the $^1\pi\sigma^*$ PES is qualitatively illustrated by the wavy line in Fig. 7(a).

The MRMP2 adiabatic energy of the $^1\pi\sigma^*$ state (calculated at its global minimum) of the PyH–NH$_3$ complex is 3.89 eV while the vertical energy (calculated at the ground state geometry) is only 4.65 eV (269 nm). These values are significantly redshifted with respect to the adiabatic energy of the PyH–water complex (4.55 eV),[27] and to the vertical energy of bare pyrrole (4.9–5.2 eV) (Refs. 28 and 29) calculated at similar level of theory.

V. DISCUSSION

Let us first summarize the experimental results:

(1) The H transfer reaction is clearly evidenced and presents a threshold around 235 nm (5.3 eV).

(2) The lifetimes of the PyH–(NH$_3$)$_n$ clusters are in the order of 10–30 ps and increase with the cluster size.

(3) The appearance time of the reaction products is similar, within the experimental uncertainty, to the decay of the parent ions.

(4) Some evaporation processes are observed since the decays depend on the cluster size distribution.

(5) From the measurements performed with the bunched picosecond laser, the cluster lifetime after evaporation is estimated to be between 1 and 10 ns.

(6) The kinetic energy of the products is fairly large and is not far from a monokinetic energy distribution as was observed for the H atoms issued from the photodissociation of PyH.[16] However in the latter case, the mean kinetic energy of the H atom was 73% of the available energy, whereas in the case of PyH–(NH$_3$)$_n$ clusters excited at 225 nm, the kinetic energy is between 0.5 and 0.6 eV for around 1.5 eV of available energy; some of the available energy must then be converted to vibrational and rotational degrees of freedom of the two radicals.

How can the H transfer mechanism be described taking into consideration the experimental results? From theoretical

calculations, the reaction should proceed only on the $^1\pi\sigma^*$ potential energy surface, this state being the lowest singlet excited state in PyH.

But the experimental observations for the reaction in clusters totally exclude a direct rupture of the N–H bond, as it seems to be the case in the free molecule. This process would lead to a very fast reaction time since a direct dissociation is expected to occur in the femtosecond range. Moreover, a much smaller kinetic energy would be released: in the free molecule excited at 243 nm, the H atom is ejected with a kinetic energy of 0.8±0.20 eV, i.e. with a 12 000 m/s velocity (the H atom velocity should be even greater—15 000 m/s—since we are exciting at 225 nm). In Ref. 16, pyrrole dissociation was studied at 243.1 nm (5.1 eV) and the dissociation threshold was estimated to be 4.02 eV, so that at this wavelength, the available energy is 1.08 eV and the H atom kinetic energy takes about 73% of the available energy. In the present work we are exciting at 225 nm (5.5 eV), the excess energy is then 1.49 eV and the H atom kinetic energy is estimated to be 73% of the available energy i.e., 1.12 eV which corresponds to a 15 000 cm^{-1} velocity. If the H atom collides with the ammonia cluster with such a high velocity, the conservation of impulsion imposes the product velocity to be in the range 240–290 m/s, 180–210 m/s, and 140–170 m/s for the NH$_4$(NH$_3$)$_2$, NH$_4$(NH$_3$)$_3$, and NH$_4$(NH$_3$)$_4$ radicals, respectively, while the measured velocities are much larger. Besides, it is hard to understand how an atom with such a velocity could be captured and stabilized by the ammonia cluster, in view of the fact that the H–NH$_3$ bond is rather weak. This seems to exclude the impulsive mechanism described in the introduction.

Additionally, the relatively long lifetime of the parent PyH–(NH$_3$)$_n$ clusters and the observed competition between reaction and evaporation imply that there is an intermediate state which is fairly deep, deep enough to allow evaporation of one ammonia unit.

This last conclusion is in part corroborated by the theoretical PES shown in Fig. 7 where two apparent minima [labeled 2 and 4 in Fig. 7(a)] separated by a barrier (3) are visible on the PES at the CASSCF level of theory. It should be noted, however, that the PES of Fig. 7(a) was obtained for the complex of pyrrole with a single ammonia molecule so that it may be applicable only for this system. So, we will use the topology of the surface presented in Fig. 7(a) only as a guide for the discussion.

It should however be noted that the dynamic electron correlation effect, largely neglected at the CASSCF level, has some influence on the shape of PES as illustrated by the single-point MRMP2 calculations presented in Table I. At this level, the barrier (3) between the 2 minima (2 and 4) vanishes so that the $^1\pi\sigma^*$ PES of the PyH–ammonia complex has very likely only one single minimum with respect to the HT reaction, a result that contradicts, at the first glance, the experimental conclusions drawn above. This apparent disagreement can be lifted when the peculiar topology of the surface is taken into account.

The electronic excitation from the ground state projects the wave packet on the $^1\pi\sigma^*$ PES near to the vertical excitation energy (structure 1). The driving force that initializes

the motion of the wave packet results from the gradient of energy near this point. Figure 7(a) shows that the gradient is largely oriented along the N–H stretching coordinate. Thus, the wave packet projected on the $^1\pi\sigma^*$ PES from the ground state starts to oscillate along the N–H stretching coordinate. At this geometry the hydrogen cannot be transferred from pyrrole to ammonia because the barrier is too large ($\Delta \approx 0.5$ eV). A barrier of this height precludes tunneling of the hydrogen atom on the time scale pertained to the experiment. In the case of the phenol ammonia complex (PhOH–NH$_3$), where the H transfer reaction likely proceeds via tunneling through a barrier of 0.5 eV,[10] the lifetime measured is 1.2 ns (at the transition origin, dropping to 390 ps when the intermolecular stretching vibration is excited), and for larger clusters ($n=2$ and 3), the lifetime decreases to $\sim$50 ps,[18] probably because the barrier to HT decreases. In contrast, the reverse is observed for PyH–(NH$_3$)$_n$ clusters, where the lifetimes increase with the cluster size. Thus, the tunneling is not expected to play an important role in PyH–(NH$_3$)$_n$ clusters, but experiments with deuterated pyrrole would settle this point.

The N–H oscillating wave packet feels a relatively small gradient in the direction of the N$\cdots$N coordinate and is expected to drift by compressing the N$\cdots$N distance. When the N$\cdots$N distance reaches a critical value of around 2.8 Å, the barrier for the ESHT reaction disappears and the wave packet can continue its motion in the direction of the global minimum (structure 4 on the surface), in the exit valley as illustrated by the wavy line in Fig. 7(a). The topology of the surface is thus expected to confine the wave packed for several N–H oscillatory periods in the entrance valley (2) before the ESHT reaction can effectively take place and the resulting product, the ammonium radical can be detected. This excited state PES bears some resemblance to the ammonia dimer (NH$_3$)$_2$ surface: in that case also a vertical excitation leads to a point where there is a substantial barrier to hydrogen transfer from (NH$_3$)$_2^*$ to NH$_4$–NH$_2$.[30] This barrier vanishes when the N–N distance decreases.[30]

To illustrate the origin of the driving force which suppresses the barrier for the HT reaction by compression of the N$\cdots$N distance and further ejects the hydrated ammonia cluster, the σ^* orbital calculated at the ground-state geometry (1), at a geometry close to the saddle point geometry (3) and at the global minimum (4) is presented in Fig. 7(b). Although the σ^* orbital is of the Rydberg nature at all these nuclear configurations, there is a substantial difference between them regarding the nodal pattern and the resulting distribution of the electronic charge. Thus the σ^* orbital populated by electronic excitation at the ground-state geometry [Fig. 7(b) (1,1$'$)] extends over the whole cluster and has a bonding nodal pattern between the particular shells localized on molecular units, with the H atom still bound to the pyrrolic nitrogen. The orbital can thus be classified as the bonding with respect to the intermolecular interaction and results in contraction of the N$\cdots$N distance. Electron transfer to the solvent occurs when the N–H distance has already lengthened to 1.2 Å and the N$\cdots$N distance shortened to 2.6 Å [Fig. 7(b), 3 and 3$'$]. At this geometry, proton transfer follows electron transfer and just neutralizes the system leading to

the ESHT reaction and the σ^* orbital localizes almost exclusively on the ammonium with an antibonding nodal pattern with respect to pyrrolyl radical [Fig. 7(b) (4,4$'$)] resulting in dissociation of the cluster. The gradient on the exit channel on the PES is relatively high, resulting in ejection of the ammonium radical with a significant kinetic energy, the force being applied between NH$_4$ and the pyrrolyl radical. This overall scheme of the reaction path corresponds to the electronic mechanism described in the Introduction. The remarkable experimental fact that a lot of kinetic energy is released in the H transfer process, with a quasimonokinetic energy distribution is qualitatively reproduced in the present calculations.

It would be very interesting to perform wave packet propagation on the PyH–NH$_3$ PES, to gain insight on the time scale of the wave packet confinement in the entrance valley.

It may be dangerous to extrapolate this PES to larger clusters, however, if the overall aspect of the PES does not change too much in the larger clusters, we can expect that some energy randomization will occur while the system is vibrating in the entrance valley. The increase in lifetime with the cluster size may reflect the higher number of degrees of freedom pertained to thermalization in a larger cluster. The same interpretation can apply to clusters which have evaporated one NH$_3$ molecule: they become colder and may stay trapped fairly long in the entrance valley, before they can find their way to the exit valley. These clusters will decay through a slow reaction process (ns) and we cannot exclude decay via another route such as radiation, intersystem crossing, or internal conversion.

A last point concerns the non-observation of any dynamics when the clusters are excited with a femtosecond laser at 200 nm (6.2 eV). Excitation at 200 nm reaches an energy region where other excited states are located, namely valence ($\pi\pi^*$) and Rydberg states of $^1A_1$ or $^1B_2$ symmetry that have high oscillator strengths and are stable with respect to dissociation along the N–H bond.[7,29]

VI. CONCLUSION

The experimental results presented here reveal that the excited state hydrogen transfer reaction in PyH–(NH$_3$)$_n$ clusters cannot be considered as a simple N–H bond rupture along a repulsive potential energy curve as first suggested by comparison with the free molecule. The results of the lifetime measurements as well as the competition between the H-atom transfer reaction and the evaporation imply that the reaction proceeds through a fairly long lived (10–30 ps), relatively deep intermediate state. The excited state PE surface calculated at the CASSCF level agrees with these conclusions: 2 minima corresponding to very different structures are apparent and the reaction path after the initial excitation can be described in four steps, first is a contraction of the N$\cdots$N distance accompanied by a vibrational motion of the pyrrolic N–H bond, then at the appropriate N$\cdots$N distance an electron transfer from PyH to the solvent occurs, immediately followed by proton transfer from PyH to ammonia, which produces the radical pair Py$^\bullet\cdots^\bullet$NH$_4$ with a very diffuse Rydberg electron cloud around the ammonium. A

strong electronic repulsion between the radicals results in the large kinetic energy release which is experimentally observed.

ACKNOWLEDGMENTS

[1] G. Pino, G. Gregoire, C. Dedonder-Lardeux, C. Jouvet, S. Martrenchard, and D. Solgadi, Phys. Chem. Chem. Phys. **2**, 893 (2000).
[2] G. Gregoire, C. Dedonder-Lardeux, C. Jouvet, S. Martrenchard, and D. Solgadi, J. Phys. Chem. A **105**, 5971 (2001).
[3] C. Dedonder-Lardeux, D. Grosswasser, C. Jouvet, and S. Martrenchard, PhysChemComm **4**, 1 (2001).
[4] S. Ishiuchi, K. Daigoku, M. Saeki, K. Hashimoto, M. Sakai, and M. Fujii, J. Chem. Phys. **117**, 7077 (2002).
[5] O. David, C. Dedonder-Lardeux, and C. Jouvet, Int. Rev. Phys. Chem. **21**, 499 (2002).
[6] H. Lippert, V. Stert, L. Hesse, C. P. Schulz, W. Radloff, and I. V. Hertel, Eur. Phys. J. D **20**, 445 (2002).
[7] A. L. Sobolewski and W. Domcke, Chem. Phys. Lett. **321**, 479 (2000).
[8] A. L. Sobolewski and W. Domcke, Chem. Phys. Lett. **315**, 293 (1999).
[9] A. L. Sobolewski, W. Domcke, C. Dedonder-Lardeux, and C. Jouvet, Phys. Chem. Chem. Phys. **4**, 1093 (2002).
[10] A. L. Sobolewski and W. Domcke, J. Phys. Chem. A **105**, 9275 (2001).
[11] R. C. Heckman, J. Mol. Spectrosc. **2**, 27 (1958).
[12] C. D. Cooper, A. D. Williamson, J. C. Miller, and R. N. Compton, J. Chem. Phys. **73**, 1527 (1980).
[13] W. M. Flicker, O. A. Mosher, and A. Kuppermann, J. Chem. Phys. **64**, 1315 (1976).
[14] J. Wan, J. Meller, M. Hada, M. Ehara, and H. Nakatsuji, J. Chem. Phys. **113**, 7853 (2000).
[15] D. A. Blank, S. North, and Y. T. Lee, Chem. Phys. **187**, 35 (1994).
[16] J. Wei, A. Kuczmann, J. Riedel, F. Renth, and F. Temps, Phys. Chem. Chem. Phys. **5**, 315 (2003).
[17] C. Dedonder-Lardeux, D. Grosswasser, C. Jouvet, S. Martrenchard, and A. Teahu, Phys. Chem. Chem. Phys. **3**, 4316 (2001).
[18] G. Gregoire, C. Dedonder-Lardeux, C. Jouvet, S. Martrenchard, A. Peremans, and D. Solgadi, J. Phys. Chem. A **104**, 9087 (2000).
[19] J. H. Glownia, G. C. Nieman, S. J. Riley, and S. D. Colson, J. Chem. Phys. **73**, 4296 (1980).
[20] B. O. Roos, Adv. Chem. Phys. **69**, 399 (1987).
[21] J. H. Nakano, Chem. Phys. **99**, 7983 (1993).
[22] M. W. Schmidt, K. K. Baldridge, J. A. Boatz *et al.*, J. Comput. Chem. **14**, 1347 (1993).
[23] K. Fuke and R. Takasu, Bull. Chem. Soc. Jpn. **68**, 3309 (1995).
[24] K. Fuke, R. Takasu, and F. Misaizu, Chem. Phys. Lett. **229**, 597 (1994).
[25] J. A. Syage, J. Phys. Chem. **99**, 7421 (1995).
[26] G. Gregoire, M. Mons, I. Dimicoli, C. Dedonder Lardeux, C. Jouvet, S. Martrenchard, and D. Solgadi, J. Chem. Phys. **112**, 8794 (2000).
[27] W. Domcke and A. L. Sobolewski, Proc. Nobel Symposium **117**, 169 (2000).
[28] H. Nakano, T. Tsuneda, T. Hashimoto, and K. Hiaro, J. Chem. Phys. **104**, 2312 (1996).
[29] M. H. Palmer, I. C. Walker, and M. F. Guest, Chem. Phys. **238**, 179 (1998).
[30] P. Farmanara, W. Radloff, V. Stert, H.-H. Ritze, and I. V. Hertel, J. Chem. Phys. **111**, 633 (1999).